NASA TECHNICAL NOTE

NASA TN D-3110

NASA TN D-3110

EXPERIMENTS TO DETERMINE ELASTIC MODULI FOR FILAMENT-WOUND CYLINDERS

by Michael F. Card

Langley Research Center
Langley Station, Hampton, Va.

NATIONAL AERONAUTICS AND SPACE ADMINISTRATION • WASHINGTON, D. C. • NOVEMBER 1965

DISCLAIMER NOTICE

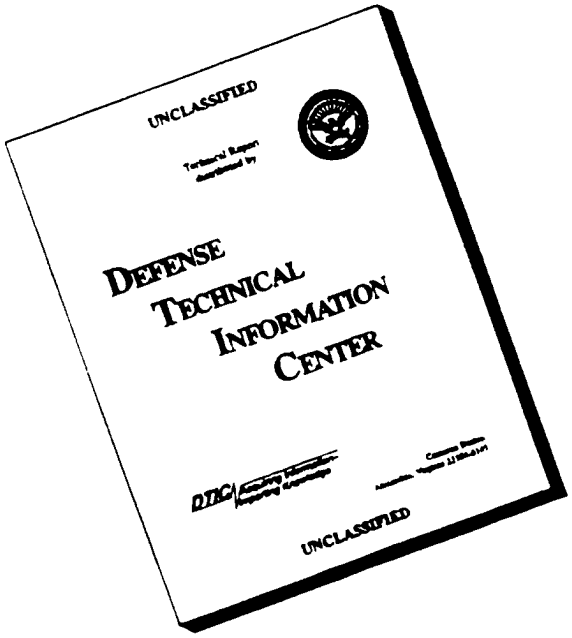

THIS DOCUMENT IS BEST QUALITY AVAILABLE. THE COPY FURNISHED TO DTIC CONTAINED A SIGNIFICANT NUMBER OF PAGES WHICH DO NOT REPRODUCE LEGIBLY.

NASA TN D-3110

EXPERIMENTS TO DETERMINE ELASTIC MODULI FOR FILAMENT-WOUND CYLINDERS

By Michael F. Card

Langley Research Center
Langley Station, Hampton, Va.

NATIONAL AERONAUTICS AND SPACE ADMINISTRATION

For sale by the Clearinghouse for Federal Scientific and Technical Information
Springfield, Virginia 22151 – Price $2.00

EXPERIMENTS TO DETERMINE ELASTIC MODULI FOR FILAMENT-WOUND CYLINDERS*

By Michael F. Card
Langley Research Center

SUMMARY

Elastic moduli for filament-wound cylinders having a wall configuration composed of several alternating helically and circumferentially wrapped layers are determined experimentally. The moduli were determined from measurements made on several glass-epoxy cylinders and tubes loaded in pressure, torsion, or compression. Computations of elastic constants were made for the test specimens as well as for hypothethical boron-epoxy cylinders to demonstrate the importance of the matrix in determining extensional stiffness. A comparison of calculations and experiment indicates that moduli measured in regions where the cylinder matrix behaves linearly are in reasonable agreement with computed values.

INTRODUCTION

As a result of the evolution of the filament-winding process, filament-wound structures are currently being evaluated for a variety of applications. The most outstanding achievement in filament winding, to date, has been the development of filament-wound casings for solid-fuel rocket motors. The present methods employed in structural design of filament-wound motor casings, however, have some serious shortcomings. The highly simplified design techniques embodied in the concept of netting analysis (ref. 1) are only valid, at best, for high internal pressure loadings. Yet, the casings, in service, are often subjected to small compressive, bending, and shear loads which can precipitate failure before internal pressurization occurs. Thus, for the designer, the ability to understand the behavior of the filamentary structure under loading conditions other than internal pressure is essential. The effects of these additional loading conditions may be estimated by reference to anisotropic shell theory. (See, for example, ref. 2.) To employ such a theory, however, a knowledge is required of the elastic constants of the structure under

*The information presented herein is based in part upon a thesis entitled "Elastic Constants for Filament-Wound Cylinders" offered in partial fulfillment of the requirements for the degree of Master of Science in Engineering Mechanics, Virginia Polytechnic Institute, Blacksburg, Virginia, June 1964.

consideration. For layered composites, values for constants associated with extension, bending, and coupling are necessary to specify the elastic properties employed in this type of theory. Only elastic constants associated with extension are considered herein.

The purpose of the present paper is to present the results of experiments made to determine the elastic moduli of filament-wound cylinders. The moduli were obtained from simple structural tests in which several multilayered glass-epoxy cylinders were loaded in pressure, torsion, or compression. The results of these tests are compared with approximate computations of elastic constants based on the work of Tsai (ref. 3) and on certain principles of orthotropic elasticity.

SYMBOLS

The units for the physical quantities in this report are given both in U.S. Customary Units and in The International System of Units (SI) (ref. 4). Appendix A presents factors relating these two systems of units.

C contiguity factor (defined in ref. 3)

D mean diameter of tube wall

E_f Young's modulus of fiber

E_m Young's modulus of matrix

E_L, E_T Young's modulus of unidirectional layer in direction parallel and perpendicular to fibers, respectively

E_x, E_y Young's modulus of cylinder wall in x- and y-directions, respectively

$\bar{E}_x, \bar{E}_y$ Young's modulus of helically wrapped layer of cylinder wall in x- and y-directions, respectively

G_f, G_m shearing modulus of fiber and matrix, respectively

G_{LT} shearing modulus of unidirectional layer

G_{xy} shearing modulus of cylinder wall

$\bar{G}_{xy}$ shearing modulus of helically wrapped layer

$$K_f = \frac{E_f}{2(1 - \mu_f)}$$

$$K_m = \frac{E_m}{2(1 - \mu_m)}$$

L	distance between station A and B (see fig. 5(b))
T	applied torque
t	thickness of cylinder wall
$\bar{t}_h$	fraction of cylinder wall thickness occupied by helically wrapped layers
v	volume fraction, ratio of constituent volume to total volume
x	surface coordinate, measured parallel to cylinder axis (see fig. 1)
y	surface coordinate, measured perpendicular to cylinder axis (see fig. 1)
α	helical wrap angle measured from axis of cylinder (see fig. 1)
γ	shearing strain
ϵ	strain
μ_f	Poisson's ratio of fiber
μ_m	Poisson's ratio of matrix
μ_L, μ_T	Poisson's ratios associated with inplane loading parallel and perpendicular to fiber direction, respectively
μ_x, μ_y	Poisson's ratios associated with extension of cylinder in x- and y-directions, respectively
$\bar{\mu}_x, \bar{\mu}_y$	Poisson's ratios associated with extension of helically wrapped layer in x- and y-directions, respectively
ρ	density of material
σ	normal stress
τ	shearing stress
ϕ	angle of tube rotation under applied torque

Subscripts:

f	fiber property
m	matrix property
L	fiber direction

T	direction transverse to fiber
x	x-direction
y	y-direction
max	maximum

EXPERIMENTAL INVESTIGATION

Test Specimens

The geometry of the filament-wound cylinders considered in this report is indicated in figure 1. The cylinder shown is constructed by wrapping filaments in alternating helically and circumferentially wrapped layers. The helically wrapped layers are composed of two half layers, with filaments oriented at angles $+\alpha$ or $-\alpha$ measured from the cylinder axis. The construction is typical of many solid-fuel rocket casings.

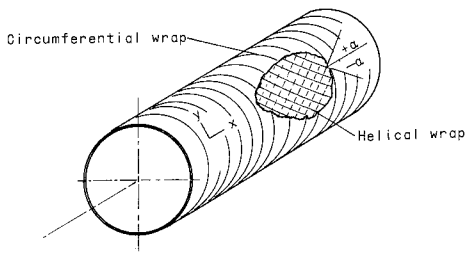

Figure 1.- Overall geometry of filament-wound cylinder.

The local geometry of the test specimens is indicated in figure 2 which is a photomicrograph of the wall section of a 15-inch-diameter (38 cm) filament-wound cylinder. The cylinder wall is composed of six alternating helically and circumferentially wrapped layers consisting of glass filaments embedded in epoxy resin. The filaments are about 3/10,000 inch (8 μm) in diameter so that there are roughly 30,000 filament sections appearing in the section shown. It is evident from figure 2 that there is considerable variation in the filament packing density in any single layer of the filament-wound cylinder.

To obtain measurements of elastic moduli, a series of simple structural tests was conducted on several filament-wound cylinders. The wall configuration of the cylinders was identical to that shown in figure 2. The test variables were the helical wrap angle α and the radius of the cylinder. The dimensions and material details of the cylinders are included in tables I, II, and III. For discussion purposes, the cylinders having a diameter of 2.6 inches (6.6 cm) will be referred to as tubes and those with a diameter of 15 inches (38 cm), as cylinders.

The values of wall thickness t, shown in tables II and III are the average of several measurements taken at random locations. The scatter in individual measurements was about ±3 percent of the value listed and was attributed to the irregular outer surface of the test specimens. The values of the volume fraction of glass v_f, listed in the tables

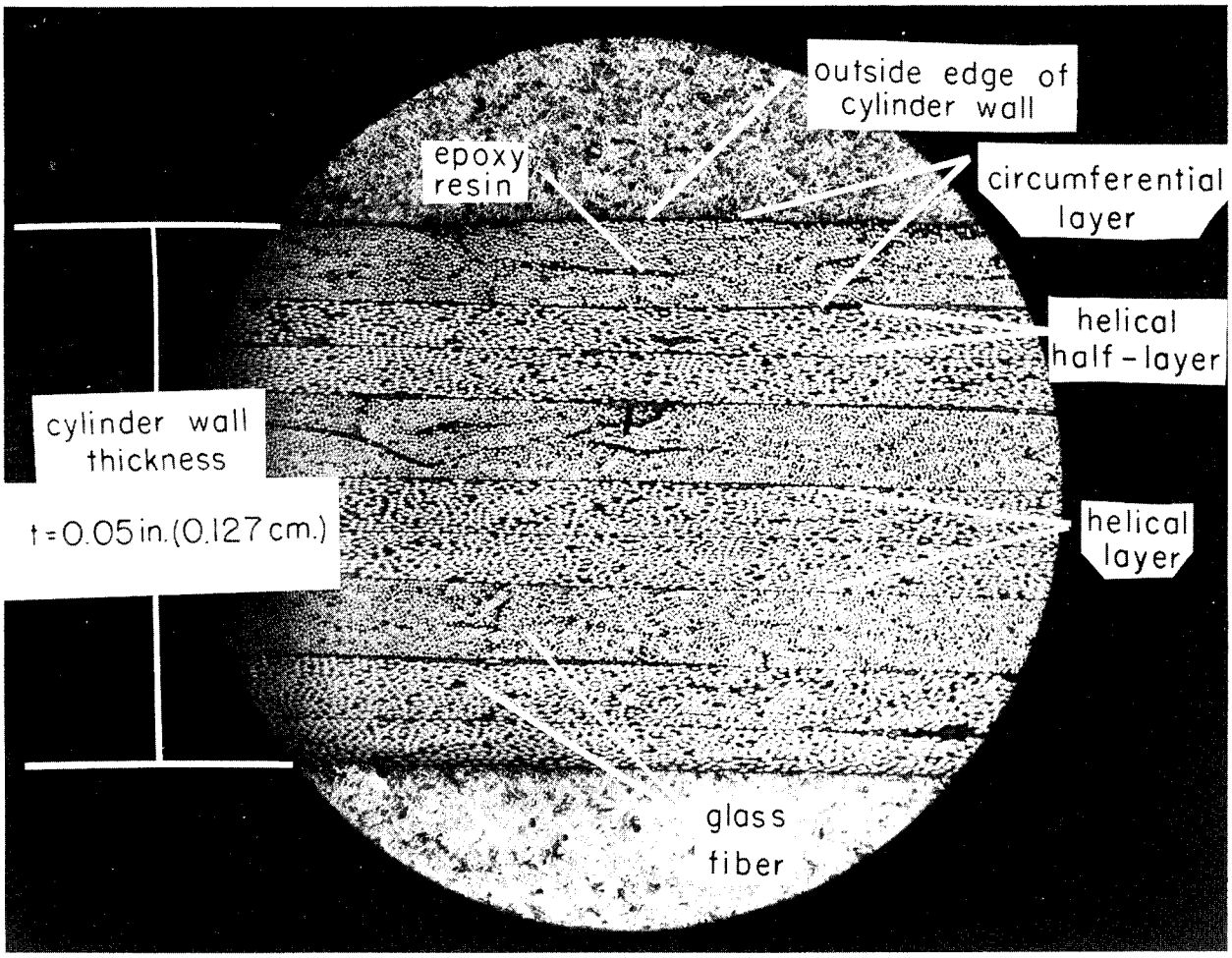

Figure 2.- Photomicrograph of wall of filament-wound cylinder.

L-65-199

were obtained from elevated-temperature tests of three or four coupons cut from the wall of each specimen. The coupons were subjected to a temperature of 1100° F (866° K) for a period of 3 hours. On the basis of some preliminary tests in which weight loss was measured continuously, the temperature and time were considered sufficient to permit virtually all the resin in the coupon to decompose. The remaining glass was weighed and the equivalent volume fraction v_f was calculated by using the values of density in table I. The scatter in calculated values of v_f was ±3 percent of the value in tables II and III.

Each of the test specimens was subjected to two types of loading to determine various elastic constants. The tubes were loaded first in torsion and then in compression whereas the cylinders were loaded first in pressure and then in compression. The magnitude of loads applied in the torsion and pressure tests were deliberately kept small to

promote linear elastic behavior of the specimens. A discussion of the individual tests is included in the following sections.

Pressurization Tests of Cylinders

To determine the circumferential modulus of the test cylinders E_y, a procedure was devised to approximate only circumferential loading in the cylinder wall by internal pressurization. The ends of the cylinders were ground flat and parallel and were then sealed between the platens of a testing machine by inserting neoprene gaskets between the ends of the cylinders and the platens. Figure 3 shows the test setup. A minimum compressive sealing load (1600 lb (7117 N)) was determined experimentally over the range of desired testing pressures. Various pressures were then applied, and at each

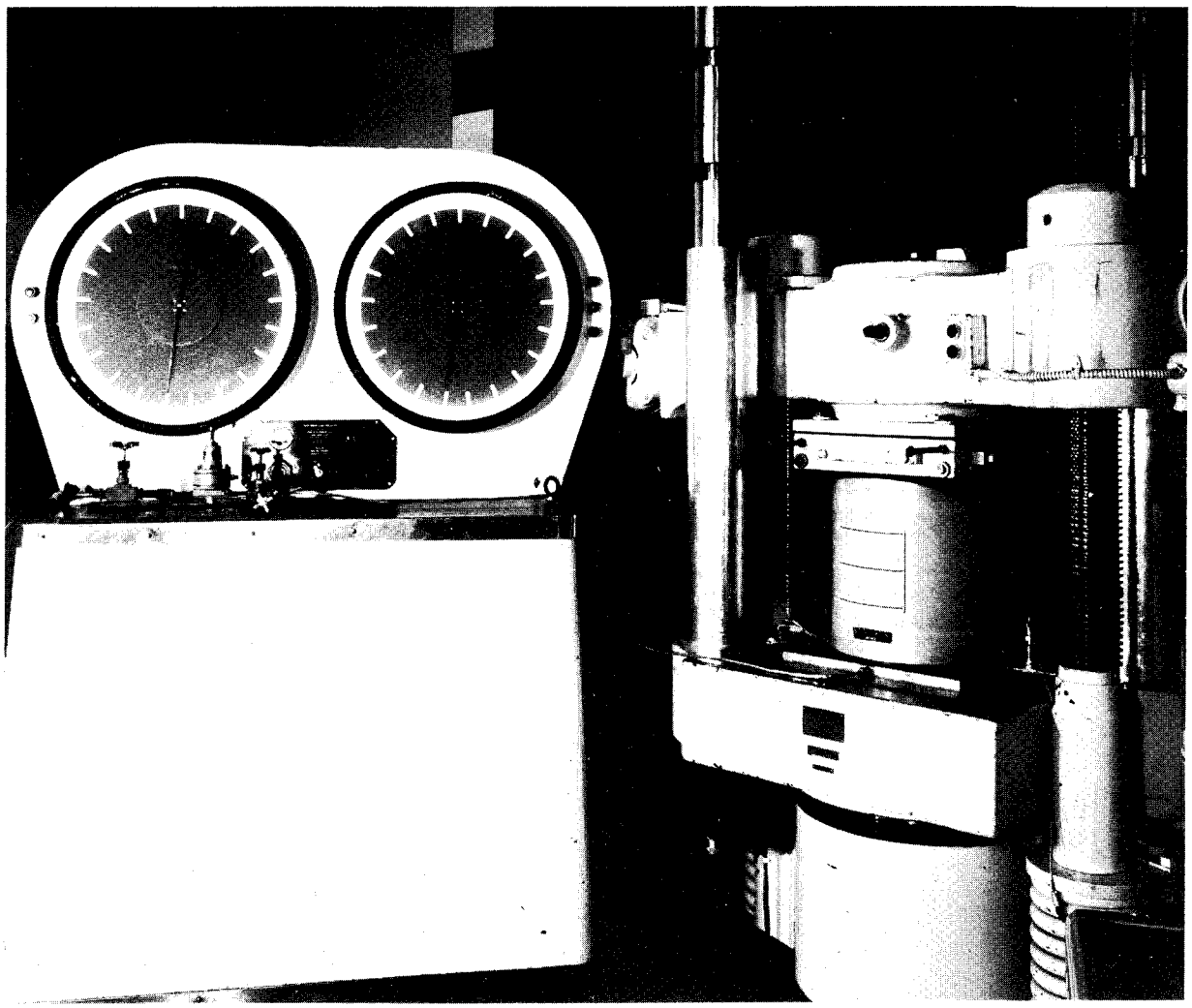

Figure 3.- Setup for pressurization tests of 15-inch-diameter (38.10 cm) cylinders. L-63-3018

pressure, enough compressive load was applied to overcome the platen loading induced by pressurization and to maintain a constant sealing load.

The procedure thus induced various circumferential tensile stresses in the wall of the cylinder together with a small, constant longitudinal compressive stress corresponding to the sealing load. The expansion of the cylinder during pressurization was measured by several 6-inch (15-cm) resistance-type, wire strain gages mounted circumferentially in back-to-back pairs on the cylinder wall. Preliminary tests with Tuckerman optical strain gages as standards indicated the acceptability of this type of measurement. An additional verification of the experimental procedure was obtained with two 7075 T-6 aluminum-alloy cylinders having the same geometry as the filament-wound cylinders. The aluminum cylinders were tested with the procedure mentioned previously; the slopes of the stress-strain curves obtained from the data were in excellent agreement with accepted values of Young's modulus.

The filament-wound cylinders were tested at various pressure levels up to a maximum internal pressure of 50 psi (345 kN/m^2). Data were recorded and reduced on a digital data recording system and the resulting stress-strain curves were found to be linear. The average slope of the circumferential stress-strain curves is presented in table II as the circumferential modulus E_y. Individual gages had a maximum deviation of $\pm 1\frac{1}{2}$ percent of the value quoted in the table.

Compression Tests of Cylinders

After completion of the pressurization tests, the cylinders were tested flat-ended in compression between the platens of a testing machine to determine the longitudinal modulus E_x. For this purpose, the cylinders had been manufactured with each end reinforced by an additional circumferential layer about $1\frac{1}{2}$ inches (3.8 cm) wide and having a thickness equal to the cylinder wall. Each cylinder was instrumented with several longitudinally oriented strain gages of the same type as those employed in the pressurization tests. During loading, the strains were recorded autographically on a 24-channel strain recorder. The overall shortening of the distance between the testing machine platens was also recorded with the use of strain gages mounted on small cantilever beams the deflection of which was equal to the travel of the platens.

The cylinders were loaded to failure. Cylinders with α equal to 25° or 45° buckled, whereas failure of cylinders with α equal to $67\frac{1}{2}^\circ$ was accompanied by buckling and splitting of the cylinder wall. Although a discussion of compressive failure is beyond the scope of this report, the maximum load that the cylinders carried is included in table II as a matter of interest. Typical stress-strain curves derived from the strain-gage data are presented in figure 4. The average of slopes faired through the linear portion of stress-strain curves similar to those shown yield the values quoted in table II

for the longitudinal modulus E_x. The load-shortening curves, obtained from the cantilever-gage data, when corrected approximately for the effects of built-up ends, were in reasonable agreement with the curves obtained from strain measurements. The scatter in values of average slope was about ±3 percent of the values in table II.

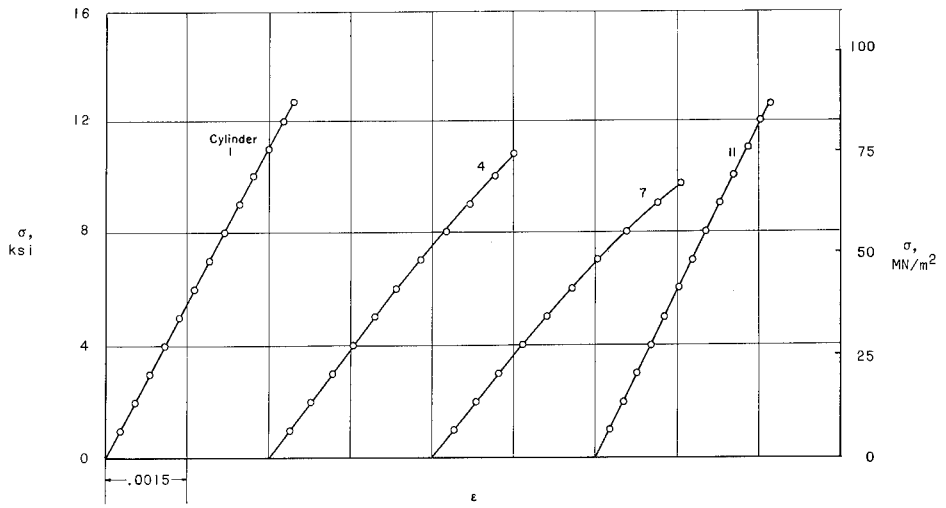

Figure 4.- Stress-strain curves for 15-inch-diameter (38.10 cm) cylinders loaded in compression.

Torsion Tests of Tubes

The filament-wound tubes were subjected to torsion in order to obtain a measure of their shearing modulus G_{xy}. The tubes were tested in the 60,000 inch-pound (6780 m · N) torsion testing machine at the Langley Research Center in which one end of the tube was held fixed and the other end, rotated to induce a moment that was measured by a sensitive weighing system. The ends of the tubes were fastened by small screws to wooden adaptor fixtures which were then bolted to the torsion machine. To measure the relative rotation of the tubes under the applied load, two steel rods were imbedded in the wall of the tube 26 inches (66 cm) apart. The rotation of the rods during testing was measured by dial gages having a sensitivity of 0.0001 inch (2.54 μm). In order to take advantage of this high sensitivity, the dial gages were fitted with a screw with which the extension of the gage spindle could be adjusted until it just touched the surface of the steel rods. Contact was detected by a simple electrical circuit. In addition to the rotational measurements, two strain rosettes were mounted on each tube to check the stress distribution. Figure 5 indicates the general features of the test setup.

All the tubes were subjected to a maximum torque of 600 in-lb (68 m · N) with the exception of tube 7 which was subjected to a maximum torque of 1200 in-lb (136 m · N). A typical curve of test results is shown in figure 6. The test results indicated that comparable curves for the remaining tubes were also linear. The values of the shearing

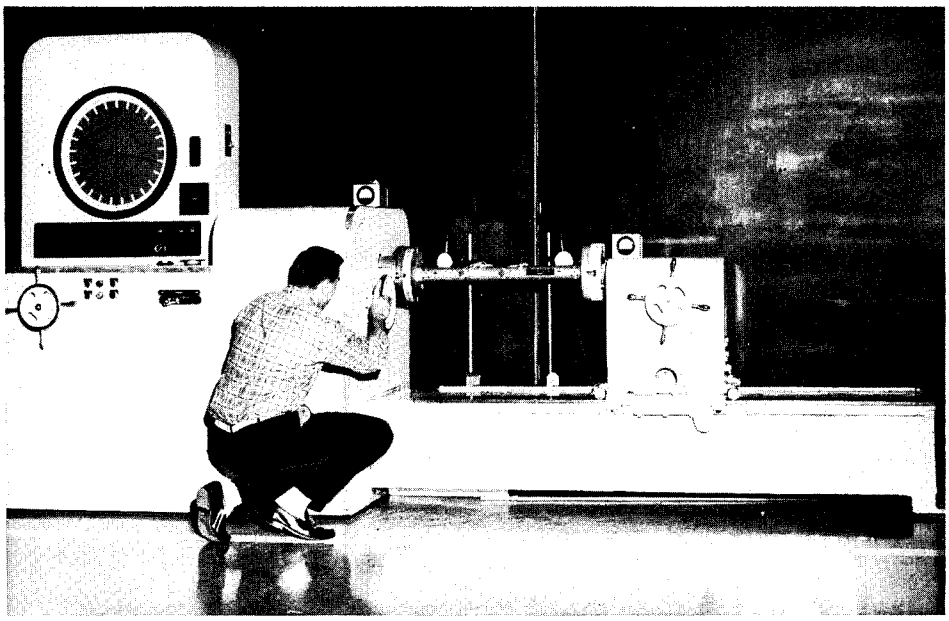

(a) Overall view. L-62-9207

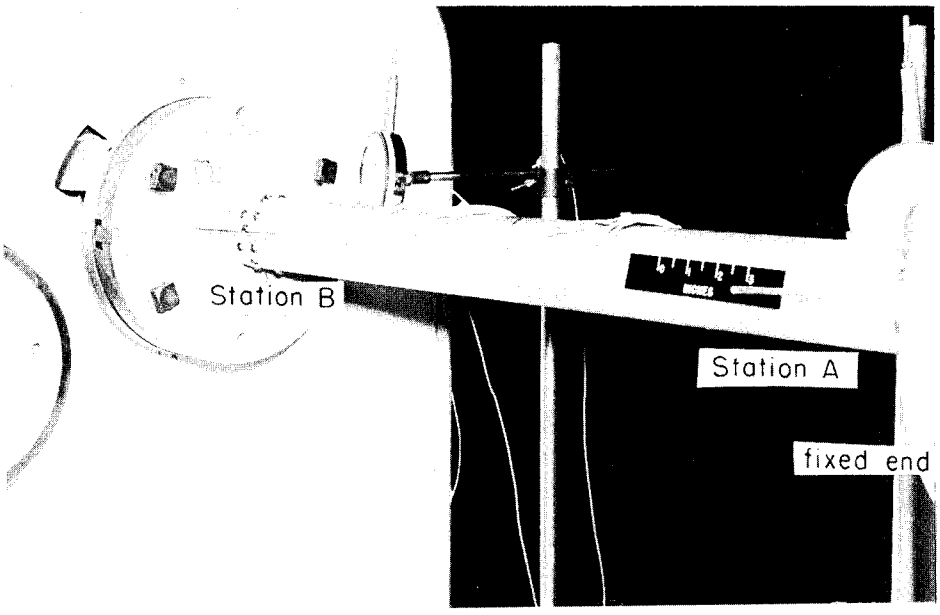

(b) Closeup view. L-62-9208.1

Figure 5.- Setup for torsion test of tube.

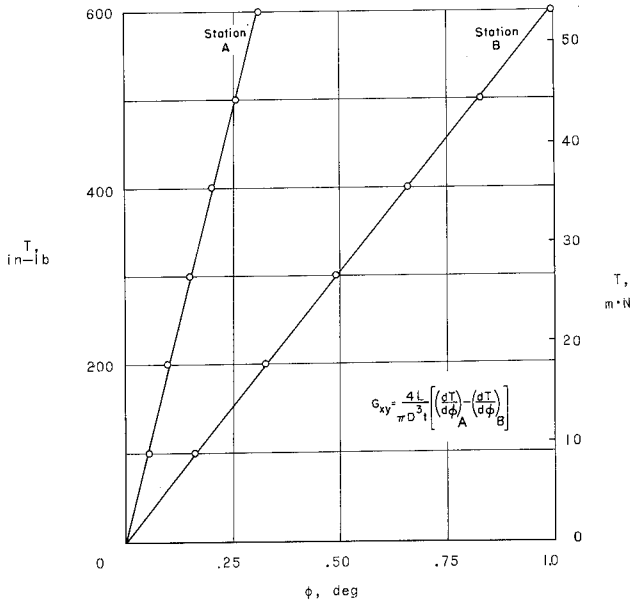

Figure 6.- Torque-twist curve obtained from torsion test of tube 5.

moduli of the tubes were obtained by computing the slope of the torque-rate-of-twist curve and converting it to a modulus by applying the classic Bredt formula to describe the relationship between torque and rate of twist. Values of the shearing modulus G_{xy} obtained from this method appear in table III. Stress-strain curves obtained from the strain-rosette data had a deviation of about $\pm 1\frac{1}{2}$ percent of the value of shearing modulus shown in the table.

Compression Tests of Tubes

After being tested in torsion, the tubes were cut into lengths suitable for compressive testing (12 inches (30.48 cm)). To prevent end failures, the ends of all the tubes except tube 8 were built up by addition of a layer of glass cloth about 1 inch (2.54 cm) wide and of thickness equal to twice that of the tube wall. The use of built-up ends was prompted by preliminary tests in which tubes 3 and 6 failed in bearing. These tubes were subsequently cut shorter and retested with built-up ends.

The ends of each tube were ground flat and parallel prior to being tested flat-ended between the platens of a testing machine. Each tube was instrumented with both an optical strain gage as well as a linear-differential-transformer strain gage located opposite each other at the middle of the tube. The tubes were then loaded to failure. During each test, the transformer gage was recorded autographically and the optical gage was used as a check on its accuracy.

The stress-strain data obtained during the tests are presented in figure 7. The data shown are the average of the strain data obtained from the two types of gages. The values of Young's modulus E_x corresponding to the slopes of the linear region of the curves are presented in table III. In addition, the maximum compressive strengths of the tubes are also presented. Failure of the tubes was accompanied by a series of splits running around the circumference of the tube.

COMPUTATION OF ELASTIC CONSTANTS

Because some of the individual layers of the cylinder wall are anisotropic and are not symmetrically oriented about its middle surface, the determination of the effective

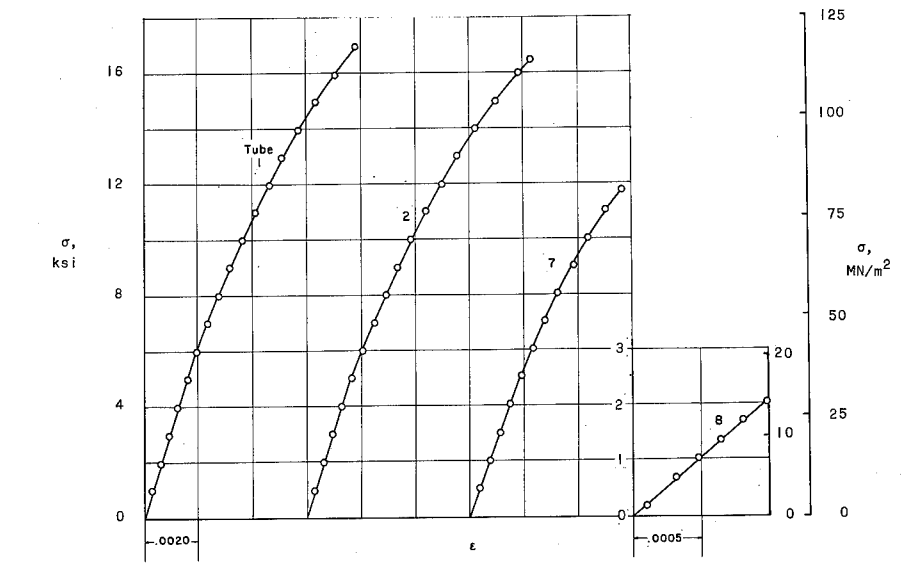

(a) α = 45, 90.

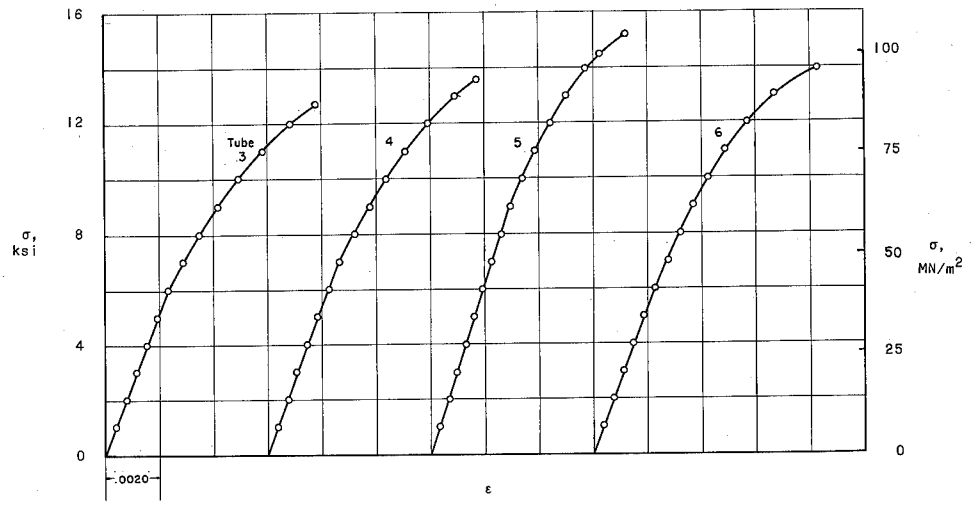

(b) $\alpha = 67\frac{1}{2}$.

Figure 7. - Stress-strain curves for tubes loaded in compression.

elastic constants of the cylinder wall is complicated. A rigorous determination of the effective constants requires solution of a complex stress-distribution problem which considers the effects of bending, extension, and coupling as well as the effects of boundary conditions at the ends of the cylinder. The effect of coupling in two-layered anisotropic plates was studied in reference 5 and found to be significant. The general equations governing the behavior of multilayered cylinders may be found in reference 2; unfortunately, solutions for the type of loading and boundary conditions employed in the present experiments are not available.

If the cylinder wall is composed of several alternating helically and circumferentially wrapped layers, the effects of antisymmetry about the wall middle surface on the behavior of the cylinder are minimized. Hence approximate methods which ignore

antisymmetry presumably would give reasonable engineering estimates of the elastic constants associated with extension. For the present computations, the cylinder wall is assumed to be composed of orthotropic layers symmetrically disposed about the middle surface of the cylinder. The two anisotropic half-layers of the helically wound portions of the cylinder wall are analytically replaced by a single orthotropic layer by employing equations found in reference 6. For multilayered composites which behave according to the aforementioned assumptions, the procedures for deriving the effective elastic constants are rather well known. (See, for example, refs. 6 to 8.) Constants for a unidirectional layer of the composite (e.g., a circumferentially wrapped layer) are computed along its principal axes of elasticity. The properties of a helically wrapped layer of the cylinder can then be obtained from the transformation equations of orthotropic elasticity for any orientation of the layer. The composite wall properties are found by integration of the constants of individual layers. A summary of the equations used to make computations of the elastic constants is given in appendix B.

Elastic constants were computed for composites having the fiber and matrix properties of the test cylinders. Descriptions of the materials and their elastic properties appear in table I. Materials 1, 2, and 3 are the glass-resin systems employed in the test cylinders. The glass properties listed are based on accepted values of the elastic constants of Type E glass fibers. The resin properties were obtained from compressive tests of a few rectangular blocks, $1 \times 1 \times 4$ inch ($2.5 \times 2.5 \times 10$ cm), constructed with the curing cycle specified. The elastic constants quoted in the table were derived from strain measurements obtained under small loads. The blocks were subsequently tested to failure to give some idea of the proportional limit of the resin. Typical stress-strain curves obtained from the failure tests are presented in figure 8. The regions much beyond the

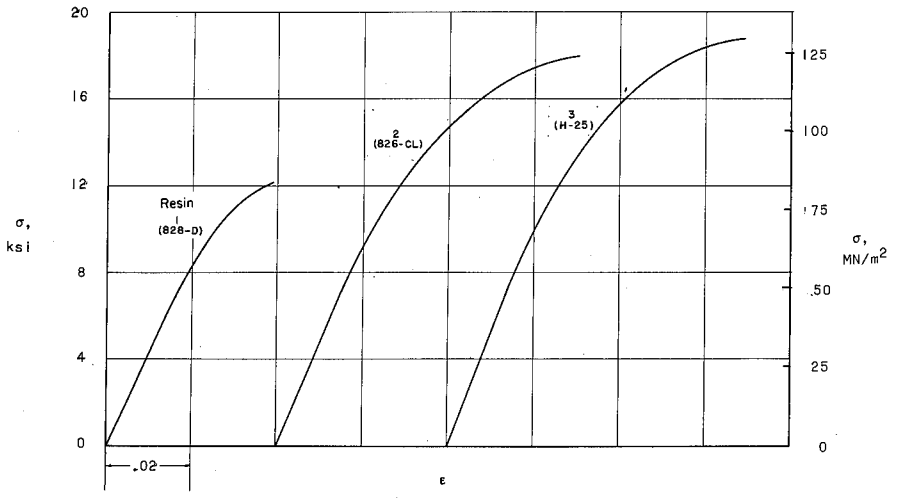

Figure 8.- Stress-strain curves for matrix. (See table I.)

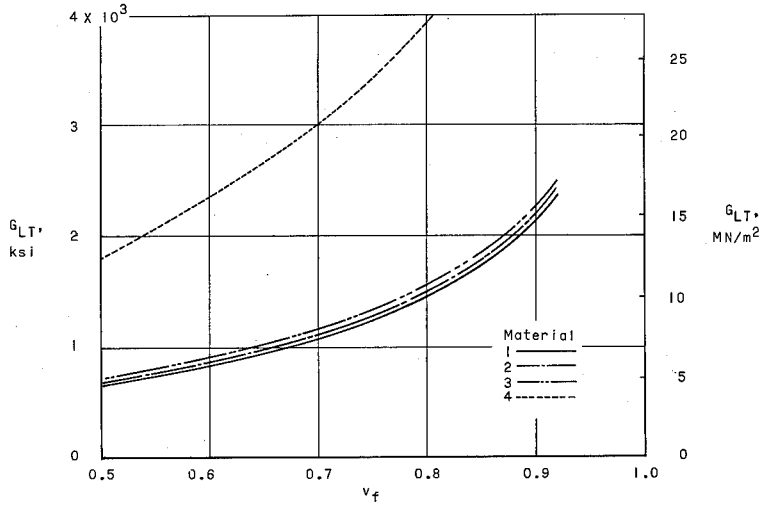

(a) Shearing modulus.

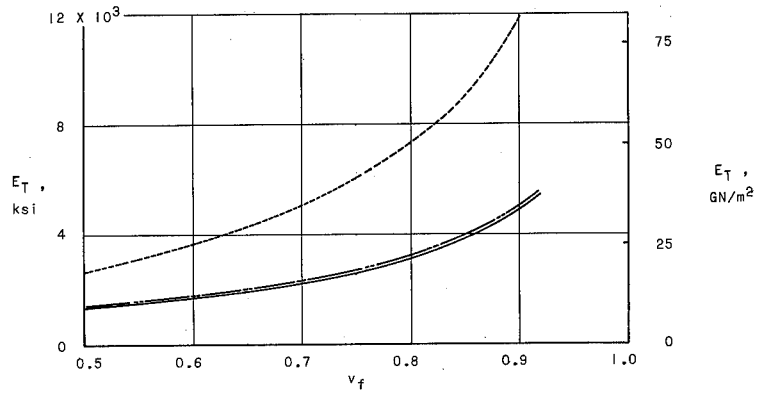

(b) Young's modulus in direction transverse to fibers.

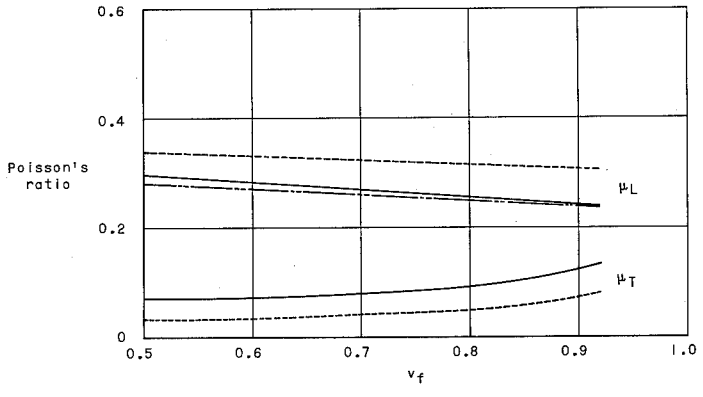

(c) Poisson's ratios associated with extension.

Figure 9.- Elastic constants for unidirectional or circumferentially wrapped layer.

proportional limit of the curves shown are influenced by instability of the block configuration as well as by the brittleness of the individual resin and should be treated accordingly.

In addition to the computations for the test cylinders, calculations were also made for composites stiffened by fibers having a relatively high Young's modulus. The material considered was a hypothetical combination of boron fibers embedded in a common epoxy resin and is indicated as material 4 in table I. Boron fibers appear to represent a significant advance in fiber technology (ref. 9) and hence their behavior in composites is of current interest.

Unidirectional Layers

Figure 9 indicates the elastic constants computed for unidirectional (or circumferentially wrapped) layers constructed from the four materials considered. The results presented include the range of fiber volume fractions usually found in filament-wound structures. The constants shown would be applicable to cylinders in which all the fibers were wrapped longitudinally or circumferentially.

Figure 9 illustrates a prevailing characteristic of

filament-wound structures. Although the matrix is selected primarily for its load-transfer capabilities, it, nevertheless, plays an important role in determining the structural stiffnesses of the composite material. For the range of volume fractions shown, figures 9(a) and 9(b) indicate that both the shearing moduli and transverse Young's moduli are considerably reduced from the fiber moduli owing to the presence of the relatively "soft" matrix. Note that an increase of five times the fiber modulus in going from glass to boron fibers does not result in a comparable change in elastic moduli of the composite over the range of volume fractions. It is only at higher volume fractions that the moduli begin to approach those of the reinforcing fibers; few manufactured filament-wound composites have a volume fraction higher than 0.785, the maximum fiber fraction achieved by square packing of circular filaments.

In making the calculations for the boron-epoxy composites, it was observed that the contiguity factor C (ref. 3) plays a much more significant part in determining the shear and transverse Young's moduli than in the case of glass-epoxy composites. Because the factor was developed for glass-epoxy structures, additional test data on composites reinforced with relatively stiff fibers are needed in order to check the generality of the

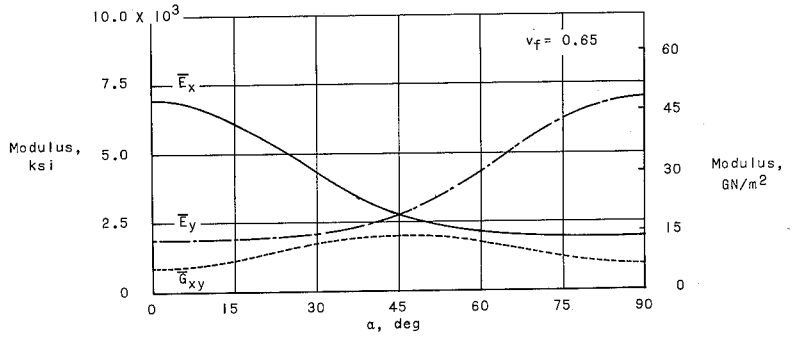

(a) Moduli; materials 1, 2, and 3.

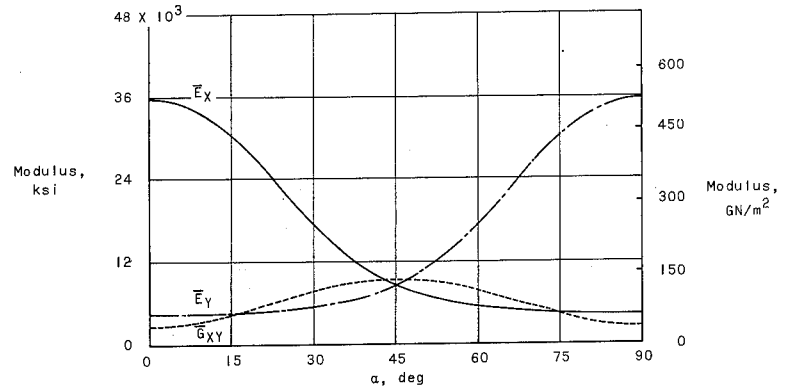

(b) Moduli; material 4.

Figure 10.- Elastic constants for helically wrapped layers.

factor. The values presented for elastic constants of boron composites should not be used without experimental verification.

Helically Wrapped Layers

Elastic constants for the helically wrapped layers of the cylinder are shown in figure 10. The effects of varying helical wrap angles are indicated for each of the four materials mentioned previously. Strictly speaking, the constants shown in the figure are valid for filament-wound cylinders having layers interspersed with fibers oriented at positive or negative α. They are used to approximate the composite behavior of the two half layers shown in figure 2. In figure 10(a), the differences in materials 1, 2, and 3 were not discernible within the plotting accuracy of the figure. Again, note the reduction in moduli of the composite from those of the reinforcing fiber as well as lack of proportionality in reduction of moduli between glass-epoxy composites and boron-epoxy composites. An interesting aspect of the helically wrapped layer is the magnitude of the Poisson's ratios $\bar{\mu}_x$ and $\bar{\mu}_y$. As shown in figures 10(c) and 10(d), the maximum values

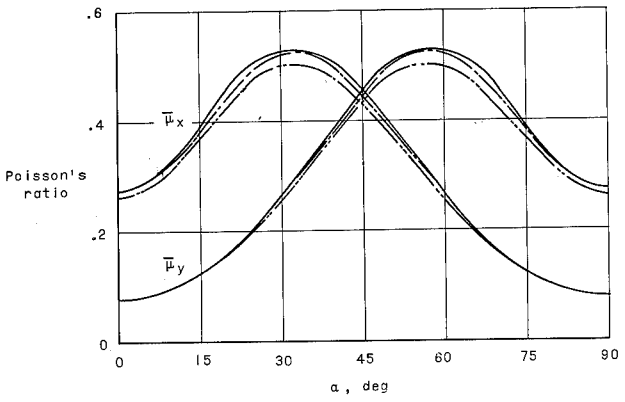

(c) Poisson's ratios; materials 1, 2, and 3.

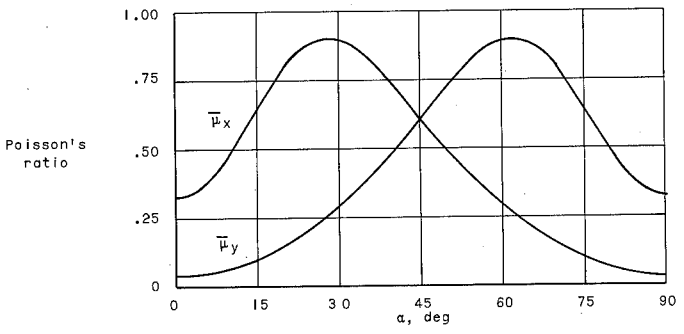

(d) Poisson's ratios; material 4.

Figure 10.- Concluded.

of Poisson's ratio are much larger than those usually associated with elastic, metallic structures. Note that the product $\bar{\mu}_x\bar{\mu}_y$ can be as large as 0.36 for a boron-reinforced composite. Thus, for certain filament-wound structures, Poisson's ratios could be expected to play an important part in determining such things as stress distribution and buckling strength. Neglecting the product $\bar{\mu}_x\bar{\mu}_y$, as is sometimes done in approximate orthotropic analyses, would appear to lead to serious inaccuracies in some instances.

COMPARISON OF COMPUTATIONS WITH EXPERIMENT

A comparison of the computed and experimentally obtained elastic moduli for the filament-wound cylinders tested is presented in figure 11. The solid curves shown were computed from equation (B9) of appendix B for the volume fractions and materials indicated in the figure and are based on the results of reference 3. In making the computations, a value of 0.60 was assigned to $\bar{t}_h$, the fraction of the total wall thickness occupied by the helically wrapped layers, on the basis of observation of photomicrographs of the walls of the test cylinders.

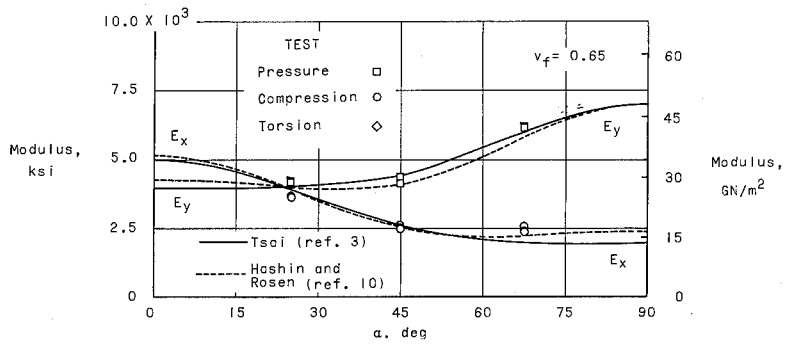

(a) Cylinders; material 1.

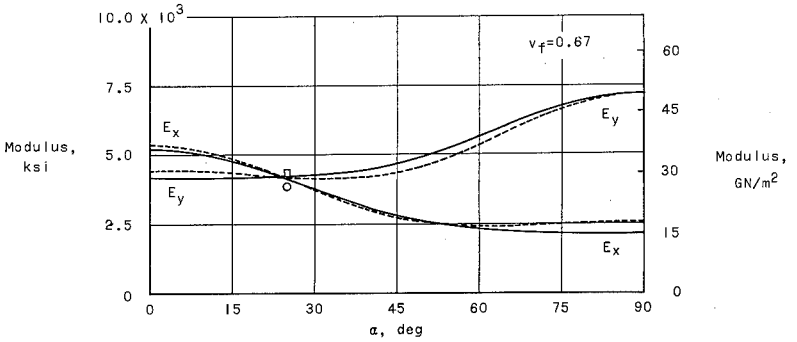

(b) Cylinder; material 2.

Figure 11.- Comparison of computations of elastic moduli with experimental results.

The dashed curves shown in figure 11 were computed by replacing equations (B2) to (B6) by comparable equations based on an analysis by Hashin and Rosen (ref. 10). The equations in the reference describing the upper bounds of elastic constants for randomly positioned fibers were employed. In making the computations, the correction to the expression for Young's modulus transverse to the fibers E_T as noted in reference 11 was incorporated. The upper and lower bounds obtained in reference 10, in fact, differ only for E_T. The choice of the upper bound was dictated by the agreement between it and experiment.

Agreement between computations and experiment is reasonably good for both cylinders and tubes. Two factors which could influence the agreement between experiment and computations are the inability to measure accurately the actual thicknesses of the individual cylinder layers as well as the actual volume fraction of filaments in each layer. The value assigned to the thickness ratio $\bar{t}_h$ is rather approximate because of the difficulty in getting a representative average measure of layer thickness from a microscopic view of the wall structure (e.g., fig. 2). Accurate volume-fraction

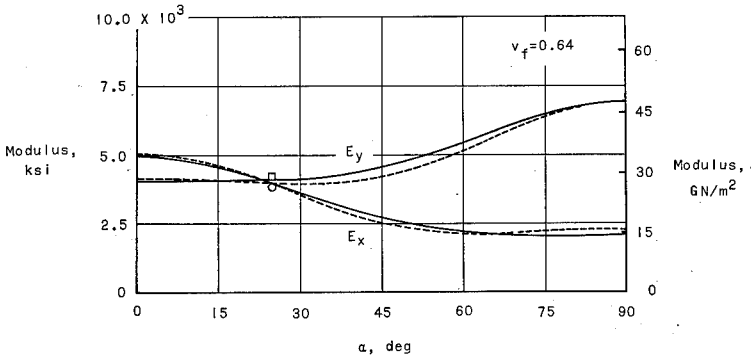

(c) Cylinder; material 3.

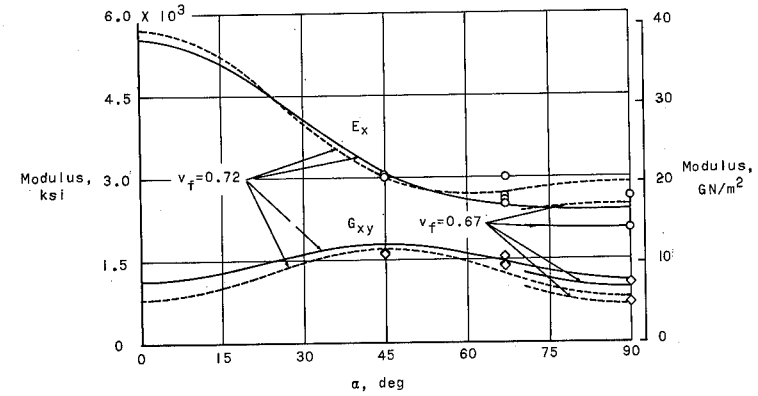

(d) Tubes; material 1.

Figure 11.- Concluded.

measurements in individual layers, of course, are even more unattainable. A third factor influencing agreement is the idealization of the cylinder wall as mentioned previously.

A limitation of the method for computing elastic constants employed herein is the requirement that the slope of the matrix stress-strain curve employed in the derivation of constituent properites be linear. Although this limitation may be construed as being rather severe, compressive test results for the 15-inch-diameter (38.1-cm) cylinders suggest that the method is valid for use in compressive buckling computations for certain cylinders of the geometry of figure 2. In figure 4, note that cylinders with a wrap angle of 25° have a linear slope up to failure; hence, computations based on linear behavior of fiber and matrix might adequately describe the structural stiffnesses necessary for buckling calculations of cylinders having this wrap angle with a radius-to-thickness ratio of about 150. The range of validity of such computations can probably be extended to cylinders with larger radius-to-thickness ratios and greater helical wrap angles since these cylinders will necessarily buckle at lower average stresses before the development of severe plasticity in the matrix.

CONCLUDING REMARKS

The results of experiments to determine the elastic moduli of several multilayered, filament-wound cylinders have been presented and discussed. Approximate computations of elastic constants were made for tested cylinders as well as for cylinders of a hypothetical material reinforced with a relatively stiff fiber to demonstrate the importance of the matrix in determining structural stiffness. Computed elastic moduli were found to be in reasonable agreement with the moduli obtained from experiment in the elastic range of the cylinder matrix.

Langley Research Center,
National Aeronautics and Space Administration,
Langley Station, Hampton, Va., August 25, 1965.

APPENDIX A

CONVERSION OF U.S. CUSTOMARY UNITS TO SI UNITS

The International System of Units (SI) was adopted by the Eleventh General Conference on Weights and Measures, Paris, October 1960, in Resolution No. 12 (ref. 4). Conversion factors for the units used herein are given in the following table:

Physical quantity	U.S. Customary Unit	Conversion factor (*)	SI Unit
Length	in.	0.0254	meters (m)
Temperature	(^{o}F + 460)	5/9	degrees Kelvin (^{o}K)
Force	lbf	4.448	newtons (N)
Density	lbm/ft^3	16.02	kilograms per cubic meter (kg/m^3)
Stress, Pressure . . .	psi=lbf/in^2	6895	newtons per square meter (N/m2)
Torque	in-lbf	0.1130	meter-newtons (m · N)

*Multiply value given in U.S. Customary Unit by conversion factor to obtain equivalent value in SI Unit.

Prefixes to indicate multiple of units are as follows:

Prefix	Multiple
kilo (k)	10^3
mega (M)	10^6
giga (G)	10^9
centi (c)	10^{-2}
micro (μ)	10^{-6}

APPENDIX B

FORMULAS FOR ELASTIC CONSTANTS

Unidirectional Layer

For an array of unidirectional fibers in a matrix, Hooke's law can be expressed as

$$\left.\begin{aligned} \epsilon_L &= \frac{1}{E_L}\sigma_L - \frac{\mu_T}{E_T}\sigma_T \\ \epsilon_T &= \frac{1}{E_T}\sigma_T - \frac{\mu_L}{E_L}\sigma_L \\ \gamma_{LT} &= \frac{1}{G_{LT}}\tau_{LT} \end{aligned}\right\} \tag{B1}$$

where L denotes a direction parallel to the fiber axes and T denotes a direction perpendicular to the fibers.

A summary of the methods available for computing the elastic constants of equation (B1) can be found in reference 12. In the present paper, the results of reference 3 were employed. The numbered equations in this section are taken directly from reference 3.

Young's modulus in the fiber direction E_L was taken as

$$E_L = v_f E_f + (1 - v_f)E_m \tag{B2}$$

where E_f and E_m are Young's moduli for the fiber and matrix, respectively, and v_f is the fiber volume fraction. (In eq. (B2) the filament misalinement factor of ref. 3 has been taken equal to unity.) Equation (B2) is an application of the so-called "law of mixtures" and has been demonstrated (refs. 3, 6, and 10) to be a good approximation to the behavior of the usual materials found in filament-wound composites.

Poisson's ratio μ_L associated with transverse strain induced by load in the fiber direction was taken as

$$\mu_L = (1 - C)\frac{K_f\mu_f(2K_m + G_m)v_f + K_m\mu_m(2K_f + G_m)(1 - v_f)}{K_f(2K_m + G_m) - G_m(K_f - K_m)(1 - v_f)}$$

$$+ C\,\frac{K_m\mu_m(2K_f + G_f)(1 - v_f) + K_f\mu_f(2K_m + G_f)v_f}{K_f(2K_m + G_f) + G_f(K_m - K_f)v_f} \tag{B3}$$

with

$$G_f = \frac{E_f}{2(1 + \mu_f)} \quad G_m = \frac{E_m}{2(1 + \mu_m)} \quad K_f = \frac{E_f}{2(1 - \mu_f)} \quad K_m = \frac{E_m}{2(1 - \mu_m)}$$

The contiguity factor C is an empirical constant to be determined from tests of unidirectional composites. A value of 0.2 was suggested in reference 3 on the basis of experiment and was adopted for the calculations presented herein.

It is interesting to note that the law of mixtures for μ_L is in reasonable agreement with equation (B3). For the range of material constants and volume fractions usually found in filament-wound structures, computations using the simple relationship

$$\mu_L = v_f\mu_f + (1 - v_f)\mu_m$$

indicate that the latter expression gives values of μ_L that deviate at most by ±5 percent from values computed from equation (B3).

Young's modulus E_T transverse to the fibers was taken as

$$E_T = 2\left[1 - \mu_f + (\mu_f - \mu_m)(1 - v_f)\right]\left[(1 - C)\frac{K_f(2K_m + G_m) - G_m(K_f - K_m)(1 - v_f)}{(2K_m + G_m) + 2(K_f - K_m)(1 - v_f)}\right.$$

$$\left. + C\,\frac{K_f(2K_m + G_f) + G_f(K_m - K_f)(1 - v_f)}{(2K_m + G_f) - 2(K_m - K_f)(1 - v_f)}\right] \tag{B4}$$

Poisson's ratio μ_T associated with strain induced by load in the direction transverse to the fiber was obtained from the reciprocal relation

$$\mu_T = E_T\frac{\mu_L}{E_L} \tag{B5}$$

The shearing modulus G_{LT} was taken as

$$G_{LT} = (1 - C)G_m\frac{2G_f - (G_f - G_m)(1 - v_f)}{2G_m + (G_f - G_m)(1 - v_f)}$$

$$+ CG_f\frac{(G_f + G_m) - (G_f - G_m)(1 - v_f)}{(G_f + G_m) + (G_f - G_m)(1 - v_f)} \tag{B6}$$

APPENDIX B

Helically Wrapped Layer

As mentioned previously, the two anisotropic half-layers in the helical layers of the cylinder are replaced by a single orthotropic layer according to the method suggested in reference 6. Constants obtained by this method are equivalent to those obtained by integrating the extensional elastic constants of two individual half-layers across their total thickness to obtain composite elastic constants associated with extension of the two-layer composite.

Hooke's law for the helically wrapped layer can then be written as

$$\left.\begin{aligned} \epsilon_x &= \frac{1}{\overline{E}_x}\sigma_x - \frac{\overline{\mu}_y}{\overline{E}_y}\sigma_y \\ \epsilon_y &= \frac{1}{\overline{E}_y}\sigma_y - \frac{\overline{\mu}_x}{\overline{E}_x}\sigma_x \\ \gamma_{xy} &= \frac{\tau_{xy}}{\overline{G}_{xy}} \end{aligned}\right\} \tag{B7}$$

where x and y correspond to the directions indicated in figure 1. The transformation equations defining the elastic constants appearing in equations (B7) can be obtained from reference 6 as

$$\left.\begin{aligned} \frac{1}{\overline{E}_x} &= \frac{1}{E_1} - m_1^2 G_{12} \\ \frac{1}{\overline{E}_y} &= \frac{1}{E_2} - m_2^2 G_{12} \\ \frac{\overline{\mu}_x}{\overline{E}_x} &= \frac{\overline{\mu}_y}{\overline{E}_y} = \frac{\mu_1}{E_1} + m_1 m_2 G_{12} \\ \frac{1}{\overline{G}_{xy}} &= \frac{1}{G_{12}} - \frac{E_1}{1 - \mu_1\mu_2}\left(m_1^2 + \mu_2 m_1 m_2\right) - \frac{E_2}{1 - \mu_1\mu_2}\left(m_2^2 + \mu_1 m_1 m_2\right) \end{aligned}\right\} \tag{B8}$$

where

$$\frac{1}{E_1} = \frac{\cos^4\alpha}{E_L} + \left(\frac{1}{G_{LT}} - \frac{2\mu_L}{E_L}\right)\sin^2\alpha\cos^2\alpha + \frac{\sin^4\alpha}{E_T}$$

$$\frac{1}{E_2} = \frac{\sin^4\alpha}{E_L} + \left(\frac{1}{G_{LT}} - \frac{2\mu_L}{E_L}\right)\sin^2\alpha\cos^2\alpha + \frac{\cos^4\alpha}{E_T}$$

APPENDIX B

$$\frac{1}{G_{12}} = \frac{1}{G_{LT}} + \left(\frac{1+\mu_L}{E_L} + \frac{1+\mu_T}{E_T} - \frac{1}{G_{LT}}\right)\sin^2 2\alpha$$

$$\frac{\mu_1}{E_1} = \frac{\mu_2}{E_2} = \frac{\mu_L}{E_L} - \frac{1}{4}\left(\frac{1+\mu_L}{E_L} + \frac{1+\mu_T}{E_T} - \frac{1}{G_{LT}}\right)\sin^2 2\alpha$$

$$m_1 = \left[\frac{\sin^2\alpha}{E_T} - \frac{\cos^2\alpha}{E_L} + \frac{1}{2}\left(\frac{1}{G_{LT}} - \frac{2\mu_L}{E_L}\right)\cos 2\alpha\right]\sin 2\alpha$$

$$m_2 = \left[\frac{\cos^2\alpha}{E_T} - \frac{\sin^2\alpha}{E_L} - \frac{1}{2}\left(\frac{1}{G_{LT}} - \frac{2\mu_L}{E_L}\right)\cos 2\alpha\right]\sin 2\alpha$$

and where α is the helical wrap angle defined in figure 1.

Composite Wall

For the alternating helical and circumferential winding configuration, the elastic constants associated with extension can be obtained from a consideration of equilibrium and compatibility conditions for the coupled layers. (See refs. 6, 7, and 8.) The resulting equations obtained for a multilayered composite having helically wrapped layers of equal thickness and circumferentially wrapped layers of equal thickness can be expressed as

$$\left.\begin{aligned}
E_x &= \frac{\overline{E}_x \bar{t}_h}{1-\overline{\mu}_x\overline{\mu}_y} + \frac{E_T \bar{t}_c}{1-\mu_L\mu_T} - \frac{\left(\frac{\overline{\mu}_x\overline{E}_y\bar{t}_h}{1-\overline{\mu}_x\overline{\mu}_y} + \frac{\overline{\mu}_T\overline{E}_L\bar{t}_c}{1-\mu_L\mu_T}\right)^2}{\frac{\overline{E}_y\bar{t}_h}{1-\overline{\mu}_x\overline{\mu}_y} + \frac{E_L\bar{t}_c}{1-\mu_L\mu_T}} \\
\mu_x &= \frac{\frac{\overline{\mu}_x\overline{E}_y\bar{t}_h}{1-\overline{\mu}_x\overline{\mu}_y} + \frac{\mu_T E_L \bar{t}_c}{1-\mu_L\mu_T}}{\frac{\overline{E}_y\bar{t}_h}{1-\overline{\mu}_x\overline{\mu}_y} + \frac{E_L\bar{t}_c}{1-\mu_L\mu_T}} \\
E_y &= \frac{\overline{E}_y \bar{t}_h}{1-\overline{\mu}_x\overline{\mu}_y} + \frac{E_L \bar{t}_c}{1-\mu_L\mu_T} - \frac{\left(\frac{\overline{\mu}_x\overline{E}_y\bar{t}_h}{1-\overline{\mu}_x\overline{\mu}_y} + \frac{\mu_T E_L\bar{t}_c}{1-\mu_L\mu_T}\right)^2}{\frac{\overline{E}_x\bar{t}_h}{1-\overline{\mu}_x\overline{\mu}_y} + \frac{E_T\bar{t}_c}{1-\mu_L\mu_T}}
\end{aligned}\right\}$$

(Equation continued on next page)

$$\mu_y = \left.\frac{\dfrac{\bar{\mu}_y \bar{E}_x \bar{t}_h}{1 - \bar{\mu}_x \bar{\mu}_y} + \dfrac{\mu_L E_T \bar{t}_c}{1 - \mu_L \mu_T}}{\dfrac{\bar{E}_x \bar{t}_h}{1 - \bar{\mu}_x \bar{\mu}_y} + \dfrac{E_T \bar{t}_c}{1 - \mu_L \mu_T}}\right\} \quad \text{(B9)}$$

with $\bar{t}_c = 1 - \bar{t}_h$ where $\bar{t}_h$ denotes the fraction of the total thickness of the cylinder wall that is occupied by the helically wrapped layers and $\bar{t}_c$ is the fraction occupied by the circumferentially wrapped layers. In making the computations reported in the text a value of 0.6 was assigned to $\bar{t}_h$.

REFERENCES

1. Shibley, Allen M.; Peritt, Harvey L.; and Eig, Merill: A Survey of Filament Winding: Materials, Design Criteria, Military Applications. PLASTEC Rept. 10, Picatinny Arsenal (Dover, N. J.), May 1962.

2. Ambartsumyan, S. A.: Theory of Anisotropic Shells. NASA TT F-118, 1964.

3. Tsai, Stephen W.: Structural Behavior of Composite Materials. NASA CR-71, 1964.

4. Mechtly, E. A.: The International System of Units – Physical Constants and Conversion Factors. NASA SP-7012, 1964.

5. Reissner, E.; and Stavsky, Y.: Bending and Stretching of Certain Types of Heterogeneous Aeolotropic Elastic Plates. Trans. ASME, Ser. E: J. Appl. Mech., Sept. 1961, pp. 402-408.

6. Greszczuk, L. B.: Elastic Constants and Analysis Methods for Filament Wound Shell Structures. Rept. No. SM-45849. Missile and Space Systems Div., Douglas Aircraft Co., Inc., Jan. 1965.

7. Dietz, Albert G. H., ed.: Engineering Laminates. John Wiley & Sons, Inc., 1949.

8. Forest Products Laboratory: Stress-Strain Relations in Wood and Plywood Considered as Orthotropic Materials. Rept. No. 1503, U.S. Dept. of Agriculture, 1962.

9. Talley, Claude P.; Clark, Wendell J.; Gunn, Kenneth M.; Wawner, Frankin E., Jr.; and Schultz, James E.: Boron Reinforcements for Structural Composites. First Summary – March 15-December 15, 1961. ASD-TDR-257, U.S. Air Force, Mar. 15, 1962.

10. Hashin, Zvi; and Rosen, B. Walter: The Elastic Moduli of Fiber-Reinforced Materials. Trans. ASME, Ser. E: J. Appl. Mech., vol. 31, no. 2, June 1964, pp. 223-232.

11. Dow, Norris F.; and Rosen, B. Walter: Evaluations of Filament-Reinforced Composites for Aerospace Structural Applications. NASA CR-207, 1965.

12. Amick, J. H.; and Nourse, J. H.: A Review of the Technical Literature for the Elastic Analysis of Filament-Wound Pressure Vessels. Rept. 1, Hercules Powder Co., July 1964.

TABLE I.- CYLINDER CONSTITUENT PROPERTIES

(a) U.S. Customary Units

Material	Resin	Curing agent	Cure		E_m, ksi	μ_m	ρ_m, lb/cu in.	Fiber	Finish	E_f, ksi	μ_f	ρ_f, lb/cu in.
			Time, hr	Temperature, ^oF								
1	EPON 828	D	2	250	450	0.40	0.043	ECG 140 (12 end)	801	10,500	0.23	0.093
2	EPON 826	CL	2	300	483	.39	.043	ECG 140 (12 end)	801	10,500	.23	.093
3	Hercules Powder Co. Formulation No. 25		3	395	510	.36	.045	ECG 140 (12 end)	801	10,500	.23	.093
4	EPON 828				450	.40		Boron		55,000	.30	

(b) International System of Units

Material	Resin	Curing agent	Cure		E_m, GN/m^2	μ_m	ρ_m, Mg/m^3	Fiber	Finish	E_f, GN/m^2	μ_f	ρ_f, kg/m^3
			Time, hr	Temperature, ^oK								
1	EPON 828	D	2	394	3.10	0.40	1.19	ECG 140 (12 end)	801	72.40	0.23	2.57
2	EPON 826	CL	2	422	3.33	.39	1.19	ECG 140 (12 end)	801	72.40	.23	2.57
3	Hercules Powder Co. Formulation No. 25		3	475	3.52	.36	1.25	ECG 140 (12 end)	801	72.40	.23	2.57
4	EPON 828				3.10	.40		Boron		379.2	.30	

TABLE II.- CYLINDER DIMENSIONS AND TEST RESULTS

(a) U.S. Customary Units

[Cylinder: inside diameter, 15.0 in.; length, 15.0 in.]

Cylinder	Material (*)	t, in.	v_f	α, deg	E_x, ksi	E_y, ksi	σ_{max}, ksi
1	1	0.0551	0.638	25	3.69×10^3	4.21×10^3	12.7
2	1	.0549	.650	25	3.75	4.20	11.9
3	1	.0551	.633	25	3.67		12.7
4	1	.0546	.632	45	2.59	4.40	10.4
5	1	.0553	.625	45	2.52	4.33	10.8
6	1	.0477	.655	45	2.67	4.17	10.4
7	1	.0557	.663	$67\frac{1}{2}$	2.44	6.20	9.7
8	1	.0540	.660	$67\frac{1}{2}$	2.42	6.19	9.1
9	1	.0552	.694	$67\frac{1}{2}$	2.61	6.20	10.0
10	2	.0505	.665	25	3.90	4.39	13.2
11	3	.0564	.639	25	3.87	4.23	12.6

*See table I.

(b) International System of Units

[Cylinder: inside diameter, 38.1 cm.; length, 38.1 cm]

Cylinder	Material (*)	t, cm	v_f	α, deg	E_x, GN/m^2	E_y, GN/m^2	σ_{max}, MN/m^2
1	1	0.1400	0.638	25	25.44	29.03	87.57
2	1	.1394	.650	25	25.86	28.96	82.05
3	1	.1400	.633	25	25.30		87.57
4	1	.1387	.632	45	17.86	30.34	71.71
5	1	.1405	.625	45	17.38	29.86	74.47
6	1	.1212	.655	45	18.41	28.75	71.71
7	1	.1415	.663	$67\frac{1}{2}$	16.82	42.75	66.88
8	1	.1372	.660	$67\frac{1}{2}$	16.69	42.68	62.74
9	1	.1402	.694	$67\frac{1}{2}$	18.00	42.75	68.95
10	2	.1283	.665	25	26.89	30.27	91.01
11	3	.1433	.639	25	26.68	29.17	86.88

*See table I.

TABLE III.- TUBE DIMENSIONS AND TEST RESULTS

(a) U.S. Customary Units

[Tube: inside diameter, 2.60 in.; Material 1.* Tube length for torsion testing, 30.0 in. Tube length for compression testing, 12 in.]

Tube	t, in.	v_f	α, deg	E_x, ksi	G_{xy}, ksi	σ_{max}, ksi
1	0.0564	0.704	45	3.07×10^3	1.61×10^3	24.8
2	.0554	.701	45	3.02	1.65	22.2
3	.0586	.709	$67\frac{1}{2}$	2.53	1.39	12.7
4	.0564	.728	$67\frac{1}{2}$	2.67	1.41	14.6
5	.0556	.728	$67\frac{1}{2}$	3.02	1.42	15.2
6	.0558	.721	$67\frac{1}{2}$	2.62	1.56	13.9
7	.0671	.721	90	2.66	1.09	12.7
8	.0709	.670	90	2.08	.74	11.0

*See table I.

(b) International System of Units

[Tube: inside diameter, 6.604 cm.; Material 1.* Tube length for torsion testing, 76.20 cm. Tube length for compression testing, 30.48 cm.]

Tube	t, cm	v_f	α, deg	E_x, GN/m^2	G_{xy}, GN/m^2	σ_{max}, MN/m^2
1	0.1433	0.704	45	21.17	11.10	171.00
2	.1407	.701	45	20.82	11.38	153.07
3	.1488	.709	$67\frac{1}{2}$	17.44	9.58	87.57
4	.1433	.728	$67\frac{1}{2}$	18.41	9.72	100.67
5	.1412	.728	$67\frac{1}{2}$	20.82	9.79	104.80
6	.1417	.721	$67\frac{1}{2}$	18.06	10.76	95.84
7	.1704	.721	90	18.34	7.52	87.57
8	.1801	.670	90	14.34	5.10	75.85

*See table I.

"The aeronautical and space activities of the United States shall be conducted so as to contribute . . . to the expansion of human knowledge of phenomena in the atmosphere and space. The Administration shall provide for the widest practicable and appropriate dissemination of information concerning its activities and the results thereof."

—NATIONAL AERONAUTICS AND SPACE ACT OF 1958

NASA SCIENTIFIC AND TECHNICAL PUBLICATIONS

TECHNICAL REPORTS: Scientific and technical information considered important, complete, and a lasting contribution to existing knowledge.

TECHNICAL NOTES: Information less broad in scope but nevertheless of importance as a contribution to existing knowledge.

TECHNICAL MEMORANDUMS: Information receiving limited distribution because of preliminary data, security classification, or other reasons.

CONTRACTOR REPORTS: Technical information generated in connection with a NASA contract or grant and released under NASA auspices.

TECHNICAL TRANSLATIONS: Information published in a foreign language considered to merit NASA distribution in English.

TECHNICAL REPRINTS: Information derived from NASA activities and initially published in the form of journal articles.

SPECIAL PUBLICATIONS: Information derived from or of value to NASA activities but not necessarily reporting the results of individual NASA-programmed scientific efforts. Publications include conference proceedings, monographs, data compilations, handbooks, sourcebooks, and special bibliographies.

Details on the availability of these publications may be obtained from:

SCIENTIFIC AND TECHNICAL INFORMATION DIVISION

NATIONAL AERONAUTICS AND SPACE ADMINISTRATION

Washington, D.C. 20546